

Wave propagation across sea-ice thickness changes

V.A. Squire^{a,*}, T.D. Williams^b

^a *Division of Sciences, University of Otago, P.O. Box 56, Dunedin, New Zealand*

^b *Department of Mathematics, University of Bristol, Bristol BS8 1TW, UK*

Received 27 July 2007; received in revised form 2 October 2007; accepted 29 October 2007

Available online 9 November 2007

Abstract

Williams and Squire (Williams, T.D., Squire, V.A., in press. The effect of submergence on wave scattering across a transition between two floating flexible plates. Wave Motion) present a mathematical theory that properly incorporates freeboard and draft, i.e. submergence, in a description of how ocean surface waves propagate across an abrupt change of properties in a continuous sea-ice cover. Typically the abrupt feature is an ice floe of different thickness from the surrounding plate, a trapped iceberg, a pressure ridge, or an open or refrozen lead. Here, we investigate how the assimilation of this floe submergence into theory alters the transmission of the wave trains, allowing the approximation and consequent limitations inherent in the majority of previous models that apply the under-ice boundary conditions at the mean open water surface to be assessed. This is done for isolated features and, using the wide-spacing approximation, for heterogeneous ice sheets made up of many such irregularities drawn from appropriate probability density distributions. It is found that the contribution associated with the underwater draft of ice floes is modest and can invariably be neglected, aside from at short periods and in heavily deformed sea-ice. While its amassed effect across the many irregular features that habitually characterize sea-ice will be significant, it is offset because of the tendency of ice covers to discourage the passage of short wavelengths preferentially by creating a background wave spectrum composed only of long period wave energy in the ice interior. More general geophysical implications are discussed, particularly in relation to global climate change and the value of ice-covered regions as a proxy for observing a warmer Earth.

© 2007 Elsevier Ltd. All rights reserved.

Keywords: Wave-ice interaction; Sea-ice; Finite draft; Green's function method; Geophysical comparison with zero draft results

1. Introduction

Ocean surface waves typically encounter many localized abrupt changes of thickness in the course of their passage through the *continuous* sea-ice of the Arctic or winter Southern Ocean, where they are often called flexural-gravity waves because of the restoring forces involved. Open or refrozen leads and polynyas, pressure ridges and dissimilar ice floes are commonplace and trapped icebergs or ice islands are also occasionally met. At each transition an impedance change occurs, resulting in partial reflection and altered wave dispersion for the transmitted portion of the wave train. Evans and Davies (1968) and Fox and

Squire (1990, 1994), for example, model how waves first pass from open water into the sea-ice plate. Barrett and Squire (1996), Squire and Dixon (2000, 2001a) and Williams and Squire (2002) consider wave propagation across one or more cracks. Squire and Dixon (2001b) and Williams and Squire (2004a) deal with what happens when waves meet an iceberg, a lead or a pressure ridge, amongst other physical configurations. The integrated effect of coming upon many heterogeneities over large distances is a gradual evolution of the wave spectrum towards longer period energy and the removal of short period waves (Squire et al., 1995). Concomitantly, when of sufficient intensity, the waves can act to fracture the sea-ice plate leading to an altered floe size distribution and changes to compaction when currents and winds are active. This potentially has an important impact on regional climate

* Corresponding author. Tel.: +64 3 479 7977; fax: +64 3 479 9045.
E-mail address: vernon.squire@otago.ac.nz (V.A. Squire).

because sea-ice affects the way the atmosphere couples to the ocean. Taken in the context of global warming it is also of immediate topical significance, as temporal adjustments in pack ice serve as a proxy of climate change (Rothrock et al., 1999; Wadhams and Davis, 2000; Comiso, 2002).

A stream of theoretical papers relating to wave propagation in sea-ice fields has been published since the Squire et al. (1995) review (see Squire, 2007), modelling both the continuous sea-ice representative of the central Arctic Ocean and the more broken-up pack ice of the marginal ice zones. Much of this work is heavily mathematical, utilizing methods from complex variable theory such as the Wiener–Hopf method and residue calculus, Green’s functions, integral equations, and variational calculus (in addition to those above, see e.g. Balmforth and Craster, 1999; Chakrabarti, 2000; Chou, 1998; Chung and Fox, 2002; Chung and Linton, 2005; Evans and Porter, 2003; Kohout and Meylan, 2006; Linton and Chung, 2003; Manam et al., 2006; Marchenko, 1997; Meylan and Squire, 1996; Meylan et al., 1997; Peter et al., 2006; Porter and Porter, 2004; Sahoo et al., 2001; Tkacheva, 2001, 2002, 2004; Williams, 2005; Williams and Squire, 2004b, 2006, 2007).

A common thread in nearly all the published theoretical work on the topic is the neglect of any draft variation associated with changes of thickness or property, so that the under-ice boundary condition is always applied at the mean open water surface. This assumption is justified by asserting that flexural-gravity wavelengths are typically an order of magnitude or more greater than the ice thickness so that effects due to the draft of floes or abrupt changes of thickness caused by refrozen leads or pressure ridges can be disregarded. While plausible, the assumption is untested and, for large pressure ridges especially, it is likely to be a source of error. This deficiency was recognized by Bennetts et al. (2007), who use a variational approach invoking the Rayleigh–Ritz method to incorporate smooth spatial changes in the submergence of continuous sea-ice, building on the work of Porter and Porter (2004). Moreover, by replacing an essential continuity condition in the Porter and Porter paper with a functional that ensures coupling of the fluid motion between the free surface and ice covered states, Bennetts et al. are able to deal with abrupt changes and, in particular, partial ice covers as well.

Williams and Squire (in press) do the same for abrupt changes in ice type by use of Green’s functions, which has the advantage that the multi-mode expansions utilized by Bennetts et al. (2007) are accommodated automatically. The method employed builds on some of the Green’s function work reported earlier in the Introduction, notably Squire and Dixon (2001b), and on Meylan (1993) where the related problem of a floating compliant raft subjected to open water waves is considered including a discussion of nonzero Archimedean draft. Although any depth is achievable, the Williams and Squire model is especially useful in deep water for features such as leads (open or refrozen), juxtaposed ice floes of different thickness, or where an

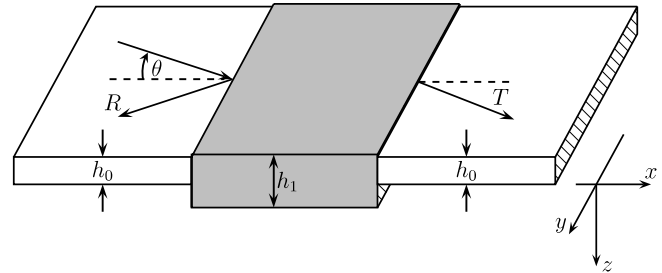


Fig. 1. A plane flexural-gravity wave arrives from the LH sea-ice plate of thickness h_0 at a central plate $x \in \mathcal{R}_1$ of thickness h_1 . (Coordinate axes are displaced to the right to avoid clutter.) Here it is partially reflected and partially transmitted into the RH plate, also of thickness h_0 . Each plate is modelled as an Euler–Bernoulli thin plate, with its underside at $\sigma_j = \rho_j h_j / \rho$. The incident wave is incident at an angle θ from normal incidence and the sea floor is at $z = H$.

iceberg becomes entrapped in surrounding sea-ice. Pressure ridges can also be modelled, despite the limited and somewhat physically unrealistic ridge profile configuration allowed (see Fig. 1). The feature, which is modelled as an Euler–Bernoulli thin plate like the sea-ice that encircles it, can be frozen to the adjacent sea-ice plate or free to move independently of it. This is important as both situations occur in nature, depending on whether freezing is occurring and on how long the arrangement has been in place under steady state conditions. When the feature is unattached to the ice around it, it will be in hydrostatic equilibrium but this will not necessarily be the case when it is welded. We have confidence in the Williams and Squire (in press) model because the mathematics is validated in a number of ways, e.g. using energy conservation, by reducing the surrounding plates to zero thickness so that they are effectively open water, and by comparison with zero-draft theories. Results in the current paper that demonstrate convergence to simpler analyses also help to corroborate the theory.

The use of a thin plate is justified by Fox and Squire (1991), who use a more sophisticated thick plate model due to Mindlin (1951) that includes the effects of rotatory inertia and transverse shear to demonstrate that thin plate theory produces excellent results except at the very shortest wavelengths or for inordinately thick ice, e.g. for ice shelves as opposed to sea-ice. Their conclusion, which is in accord with Mindlin (1951), is that the plate thickness must be more than one tenth of the wavelength for substantial differences to occur between the two methods. Regardless, in typical sea-ice such discrepancies only occur at extremely short periods, where waves will be totally reflected from any feature in the ice that they encounter. Accordingly, we rest content that the thin plate model is effective for the problem being studied.

While the context of this paper is geophysical, a complementary corpus of work exists in the marine engineering literature concerned with how an isolated body or a finite number of bodies in an otherwise unbounded fluid reacts to an ocean wave train. Textbooks by Newman (1977), Sarpkaya and Isaacson (1981) and Linton and

McIver (2001) each provide a comprehensive description of the field. In many cases, floating bodies are taken to be rigid – as opposed to flexible, but the effect of draft is correctly incorporated. The hydroelastic approach herein is less common but some cognate studies do exist that either

- extend into hydroelasticity applications the conventional methods of seakeeping analyses that separate the problem into its diffraction and radiation components (see Newman, 1994) and use a linear superposition of the dry modes of the floating structure formulated in terms of principal coordinates associated with those modes (Bishop and Price, 1979; Bishop et al., 1986), or
- utilize so-called direct methods (Eatock Taylor, 2003, 2007) that relate primarily to the behaviour of a solitary pontoon-type VLFS (very large floating structure) such as a floating airport, mobile offshore base or compliant breakwater subjected to waves in an ocean of infinite expanse (see e.g. Meylan, 1993; Wu et al., 1995; Andrianov and Hermans, 2005; Hermans, 2007).

These works differ from the arguably mathematically more demanding situation described in Williams and Squire (in press) and applied in the current paper, where the ocean surface is not free (see Fig. 1), notwithstanding the mathematical link observed above to Meylan (1993).

In Section 2, a brief commentary on the model is provided for thoroughness; the interested reader is referred to Williams and Squire (in press) for the complete mathematical development. Some results for isolated features and combinations of features are given in Section 3, followed by a discussion of the geophysical implications in Section 4.

2. The model

2.1. Problem

Fig. 1 shows the configuration being modelled. A plane flexural-gravity wave travels from the left into a plate of different thickness, where it is partially reflected and partially transmitted into the right hand region. Properties are designated using the subscript $j=0$ in the outer regions ($x \in \mathcal{R}_0 : -\infty < x < 0, l < x < \infty$) and $j=1$ for the central plate ($x \in \mathcal{R}_1 : 0 \leq x \leq l$), so the flexural rigidities and drafts of each plate are, for example, $D_j = E_j h_j^3 / 12(1 - \nu_j^2)$ and $\sigma_j = \rho_j h_j / \rho$, where E_j , ν_j and ρ_j are the Young's modulus, Poisson's ratio and density of the plate in the j th region, while ρ is the (constant) water density. The lower surfaces of each plate are located at $z = \sigma_j$.

If, as well as a constant fluid density, we assume that the fluid beneath the plates is inviscid and that flow is irrotational, a potential function $\Phi(x, y, z, t)$ exists such that the velocity $(u, v, w)^T$ of a fluid particle is given by $\nabla\Phi$. Since the incident wave forcing is periodic in time and the geometry of the problem is shift-invariant in the y direction, Φ has the form

$$\Phi(x, y, z, t) = -Re[i\phi(x, z)e^{i(\alpha_y y - \omega t)}], \quad (1)$$

where if ω , θ and γ_0 are the radial frequency, angle of incidence and wave number of the incident wave, $\alpha_y = \gamma_0 \sin \theta$. The $-i$ factor is added for convenience and γ_0 is related to ω by the dispersion relation for the ice with thickness h_0 .

After choosing an integer m such that $h_m = \max\{h_0, h_1\}$ and non-dimensionalizing all lengths with respect to a natural length $L = (D_m / \rho \omega^2)^{1/5}$, and flexural rigidities with respect to D_m , the system that ϕ must satisfy is

$$(\nabla^2 - \alpha_y^2)\phi(x, z) = 0, \quad (2a)$$

$$\mathcal{L}_j(\partial_x)\chi(x) + \phi(x, \sigma_j) = 0 \quad \text{for } x \in \mathcal{R}_j, \quad (2b)$$

$$\phi_z(x, H) = 0, \quad (2c)$$

$$\phi_x(x_e, z) = 0 \quad \text{for } z \in (\sigma_0, \sigma_1), \quad (2d)$$

where $x_e \in \{0, l\}$, $\mathcal{L}_j(\partial_x) = D_j(\partial_x^2 - \alpha_y^2)^2 + \lambda - \sigma_j$, $\lambda = g/(L\omega^2)$, $\chi(x) = \phi_z(x, \sigma_j)$ for $x \in \mathcal{R}_j$, and $j = 0, 1$. The constant g in the parameter λ is the acceleration due to gravity, which is taken to be 9.81 ms^{-2} . Eq. (2b) is the non-dimensional form of the thin plate equation, which requires the difference between the air and water pressures on the plate to be balanced by the strain in the plate. Note that the effect of added mass and added damping is included in (2), as they enter through the dynamic pressure which includes hydrostatic effects (Eatock Taylor, 2007). (see Williams and Squire, in press, for a fuller derivation.)

A flexible central plate must also satisfy some conditions at its ends $x_e \in \{0, l\}$. When it is free to move independently of the two outer plates or when $h_0 = 0$, χ will satisfy

$$D(x_e^\pm)\mathcal{L}_-(\partial_x)\chi(x_e^\pm) = 0, \quad (3a)$$

$$D(x_e^\pm)\mathcal{L}_+(\partial_x)\chi'(x_e^\pm) = 0, \quad (3b)$$

where $D(x) = D_j$ for $x \in \mathcal{R}_j$ and $\mathcal{L}_\pm(\partial_x) = (\partial_x^2 - \alpha_y^2) \mp (1 - \nu)\alpha_y^2$. If, on the other hand, adjacent plates are frozen or welded together, χ will satisfy

$$\chi(x_e^-) = \chi(x_e^+), \quad (4a)$$

$$\chi'(x_e^-) = \chi'(x_e^+), \quad (4b)$$

$$D(x_e^-)\mathcal{L}_-(\partial_x)\chi(x_e^-) = D(x_e^+)\mathcal{L}_-(\partial_x)\chi(x_e^+), \quad (4c)$$

$$D(x_e^-)\mathcal{L}_+(\partial_x)\chi'(x_e^-) = D(x_e^+)\mathcal{L}_+(\partial_x)\chi'(x_e^+). \quad (4d)$$

Conditions (3) and (4) effectively imply that energy is conserved at each edge, i.e. no translational or rotational work is done on or by any of the edges. Also note the effect that differences in the thicknesses on each side of each edge have on conditions (4c) and (4d) due to the presence of the rigidity terms $D(x_e^\pm)$.

In addition, Φ must satisfy appropriate radiation conditions that force it to behave like a combination of a unit incident wave and a reflected wave of amplitude R as $x \rightarrow -\infty$, and a transmitted wave of amplitude T as $x \rightarrow \infty$. In terms of ϕ

$$\phi(x, z) \sim \begin{cases} (e^{i\alpha_y x} + R e^{-i\alpha_y x})\phi(z, \gamma_0) & \text{as } x \rightarrow -\infty, \\ T e^{i\alpha_y x}\phi(z, \gamma_0) & \text{as } x \rightarrow \infty, \end{cases} \quad (5)$$

where $\varphi(z, \gamma) = \cosh \gamma(z - H) / \cosh \gamma(\sigma_0 - H)$, γ_0 is the real wave number that satisfies the dispersion relation

$$f_0(\gamma) = (D_0\gamma^4 + \lambda - \sigma_0)\gamma \tanh \gamma(H - \sigma_0) = 0$$

$$\text{and } \alpha_0 = \sqrt{\gamma_0^2 - \alpha_y^2} = \gamma_0 \cos \theta.$$

2.2. Solution

When $h_1 \geq h_0$, the following three steps summarize the method of solution employed:

- (1) Green’s theorem is used to derive an integral representation of ϕ in terms of its own value and that of its normal derivative on the surfaces Γ of the central plate that are exposed to the underlying fluid. The Green’s function that we use to do this is presented below.
- (2) The normal derivative of ϕ is eliminated from this integral representation, allowing us to write the potential entirely in terms of its own values when $(x, z) \in \Gamma$. This is straightforward on the vertical segments of Γ but it is slightly more difficult on the horizontal part where we use a variation of the method of [Meylan and Squire \(1994\)](#) and invoke a second Green’s function.
- (3) A resulting integral equation is solved, incorporating any necessary edge conditions.

When $h_1 < h_0$, we must approximate R and T using the method described in Section 2.3 (for reasons given by [Williams and Squire, in press](#)).

2.2.1. Primary Green’s function

The Green’s function is found using the method of [Evans and Porter \(2003\)](#), i.e. the Fourier transform of an analogous system to Eq. (2) is written down, solved and inverted using Cauchy’s residue theorem to give

$$G(x - \xi, z, \zeta) = i \sum_{\gamma \in S_0} A(\gamma) e^{i\alpha|x-\xi|} \varphi(z, \gamma) \varphi(\zeta, \gamma), \tag{6}$$

where $\alpha(\gamma) = \sqrt{\gamma^2 - \alpha_y^2}$, chosen so that $\text{Arg}[\alpha] \in [0, \pi)$,

$$A(\gamma) = -A_0^2(\gamma)\gamma^2 / \alpha(H(A_0^2\gamma^2 - 1) + 5D_0\gamma^4 + \lambda - \sigma_0),$$

and $A_0(\gamma) = \mathcal{L}_0(i\alpha)$.

The set S_0 contains the roots of the dispersion relation $f_0(\gamma) = 0$ with arguments taken from $[0, \pi)$. These roots are distributed throughout the complex plane as shown by [Fox and Squire \(1990\)](#). As $|\gamma| \rightarrow \infty$, the roots $\gamma \rightarrow in\pi / (H - \sigma_0)$ for a positive integer n so $A(\gamma) \sim -1/in\pi$. Consequently, the series (6) fails to converge at $(\xi, \zeta) = (x, z)$ and is slow to converge when the two points are close together. The situation with the normal derivative of G is even worse, as it never converges when $x = \xi$. This is alleviated by writing the series in an alternative absolutely convergent form with the singularities isolated as explicit logarithmic terms ([Williams and Squire, in press](#)). Alternatively, if the water depth is large enough and the incoming waves are normally inci-

dent, the infinite depth Green’s function may be used, for which there is an analytical expression ([Meylan and Squire, 1994](#); [Squire and Dixon, 2001b](#); [Williams and Squire, in press](#)).

2.2.2. Secondary Green’s function

To derive an integral relationship between $\chi(x)$ and $\phi(x, \sigma_1)$, a second Green’s function g satisfying

$$\mathcal{L}_1(\partial_\xi)g(x - \xi) = -\delta(x - \xi), \tag{7}$$

and certain conditions as $|x - \xi| \rightarrow \infty$ is used. By use of Fourier transforms, g is found to be

$$g(x) = -\frac{1}{2\pi} \int_{-\infty}^{\infty} \frac{e^{i\alpha|x|}}{D_1\gamma^4 + \lambda - \sigma_1} d\alpha = -i \sum_{n=0}^1 \frac{e^{ik_n|x|}}{4k_n\kappa_n^2} \text{ for } \lambda \neq \sigma_1. \tag{8}$$

In Eq. (8) $\kappa_n^4 = -(\lambda - \sigma_1) / D_1$, $\text{Arg}[\kappa_0] \in [0, \pi/2)$ and $\kappa_1 = i\kappa_0$, and $k_n = \sqrt{\kappa_n^2 - \alpha_y^2}$, where $\text{Arg}[k_n] \in [0, \pi)$ for $n = 0, 1$. Corresponding expressions when $\lambda = \sigma_1$ are given by [Williams and Squire \(in press\)](#) but this occurs very rarely and is in fact dealt with numerically by another method.

2.2.3. Integral equation

The integral equation

$$\chi(x) = \int_0^l g(x - \xi)\phi(\xi, \sigma_1) d\xi + \mathcal{L}_{\text{edge}}^T(\partial_x)(P_0^+g(x) - P_l^-g(x - l)), \tag{9}$$

where

$$\mathcal{L}_{\text{edge}}(\partial_x) = - \begin{pmatrix} \mathcal{L}_+(\partial_x)\partial_x \\ \mathcal{L}_-(\partial_x) \\ \partial_x \\ 1 \end{pmatrix} \text{ and } P_{x_e}^\pm = \lim_{x \rightarrow x_e^\pm} D(x) \begin{pmatrix} 1 \\ \partial_x \\ \mathcal{L}_-(\partial_x) \\ \mathcal{L}_+(\partial_x)\partial_x \end{pmatrix} \chi(x),$$

is found by multiplying Eq. (2b) by $g(x - \xi)$ and then integrating by parts. Again it is possible that $\lambda = \sigma_1$; here this is dealt with by solving a slightly amended version of Eq. (7).

This allows us to eliminate χ from the following integral equation, which was obtained by using the primary Green’s function G :

$$\phi(x, z) = \mathcal{L}_{\text{edge}}^T(\partial_x)(P_l^+G(x - l, z, \sigma_0) - P_0^-G(x, z, \sigma_0)) + e^{i\alpha_0 x} \varphi(z, \gamma_0) + \int_0^l G(x - \xi, z, \sigma_1)\chi(\xi) d\xi$$

$$\begin{aligned}
 & - \int_0^l G_\zeta(x - \zeta, z, \sigma_1) \phi(\zeta, \sigma_1) d\zeta \\
 & + \int_{\sigma_0}^{\sigma_1} G_\zeta(x, z, \zeta) \phi(0, \zeta) d\zeta \\
 & - \int_{\sigma_0}^{\sigma_1} G_\zeta(x - l, z, \zeta) \phi(l, \zeta) d\zeta.
 \end{aligned} \tag{10}$$

The $P_{x_c}^\pm$ are unknown constants that are eliminated by applying the appropriate edge conditions.

2.3. Wide spacing approximation

In Section 3, we will also present some results that arise from a wide spacing approximation, which is used in two ways that each follow from the same general formula. The first way treats the scattering by two features of which either may be a ridge or a lead, and the second approximates the scattering by a single lead as we are unable to calculate it exactly when submergence is allowed for (Williams and Squire, in press). We only show lead results when $h_1 = 0$, as the wide spacing approximation is accurate even for extremely small lead widths (Vaughan et al., 2007; Williams, 2005).

Let the first scatterer (which may be a ridge, lead or an abrupt jump in ice thickness like the edge of a lead) have reflection and transmission coefficients R_0 and T_0 and have its left hand limit located at $x = 0$. Also let the second scatterer have reflection and transmission coefficients R_1 and T_1 and have its left hand limit at $x = d$. The ice to the right and left of the two scatterers is taken to have thickness h_0 , while the ice bounded between them is taken to have thickness h_2 . This ice will have corresponding real wave number γ_2 , which satisfies the dispersion relation

$$f_2(\gamma) = (D_2\gamma^4 + \lambda - \sigma_2)\gamma \tanh \gamma(H - \sigma_2) = 0,$$

where $D_2 = (h_2/h_m)^3$, $\sigma_2 = \sigma_m(h_2/h_m)$ and the subscript m relates to $\max\{h_0, h_2\}$ in the manner of Section 2.1.

Assuming that any evanescent waves that are produced by the first scatterer have decayed to insignificance by the time they reach the second, the two objects combined will have scattering coefficients

$$R = R_0 + \frac{R_1 T_0 \check{T}_0 e^{2i\alpha_2 d}}{1 - \check{R}_0 R_1 e^{2i\alpha_2 d}}, \tag{11a}$$

$$T = \frac{T_0 T_1 e^{i(\alpha_2 - \alpha_0)d}}{1 - \check{R}_0 R_1 e^{2i\alpha_2 d}}, \tag{11b}$$

where $\alpha_2 = \sqrt{\gamma_2^2 - \alpha_y^2}$, $\check{R}_0 = -R_0^* T_0 / T_0^*$ and $\check{T}_0 = (1 - |R_0|^2) / T_0^*$ are the scattering coefficients corresponding to a wave arriving at the first scatterer from the right as opposed to the left. Eq. (11) were originally derived by Kreisel (1949).

To approximate the scattering by a pair of features (ridges/leads) from (11), we set $h_2 = h_0$ (making $\alpha_2 = \alpha_0$) and take the first scatterer to be the left hand feature and the second one to be the right hand one. On the other hand, to approximate the scattering by a single lead then we set $h_2 = h_1$ and $\alpha_2 = \alpha_1$. In this case, R_0 and T_0 correspond

to the scattering of a wave travelling beneath a sheet of ice with thickness h_0 by an abrupt transition into ice of thickness h_1 , while $R_1 = \check{R}_0$ and $T_1 = \check{T}_0$. These coefficients are approximated as described by Williams and Squire (in press).

In Section 3, we seek to estimate the scattering by a field consisting of many (50–1000) features. Although Eq. (11) can easily be extended iteratively to any number of features, we would like to eliminate its dependence on the separations of adjacent features (through the parameter d). Consequently, following Williams and Squire (2004a) we note that $|T|^2$, as given by (11), is periodic in d and average over one period to give

$$\frac{1}{2\pi} \int_0^{2\pi} |T|^2 dt = \frac{|T_0 T_1|^2}{1 - |R_0 R_1|^2}, \tag{12}$$

where $t = 2\alpha_2 d$. Because the denominator is usually quite close to 1, we may neglect it to obtain the so-called serial approximation

$$|T| = |T_0 T_1|. \tag{13}$$

This was shown by Williams and Squire (2004a) to approximate the median value of $|T|$ well, and we confirm this in Section 3. It is noteworthy that by taking the logarithm of $|T|^2$ before averaging, Berry and Klein (1997) obtained the formula (13) without making any further approximations.

3. Results

Throughout this section, we use the following physical parameters for the sea-ice and the water beneath: $E_j = 5 \text{ GPa}$, $\nu_j = 0.3$, $\rho = 1025 \text{ kg m}^{-3}$, $\rho_j = 0.9\rho$. The various curves of Figs. 2 and 3 provide a comparison between no submergence and the case where the draft of the sea-ice

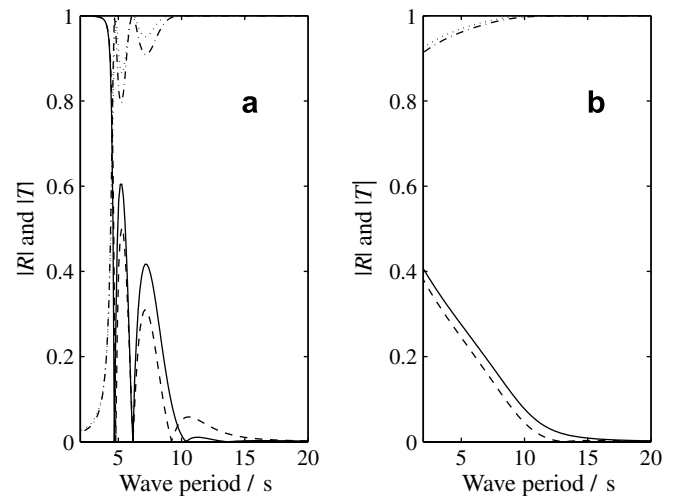


Fig. 2. Scattering by a 20×2 -m-thick floe embedded in 1 m sea-ice floating on deep water. The solid and dash-dot curves, denoting R and T , respectively, assimilate the effect of the (Archimedean) draft while the dashed and dotted curves, again for R and T , are for no submergence. The curves in part (a) are for the free edge case (3), while those in (b) are for when the floe is welded to the surrounding ice sheet (4).

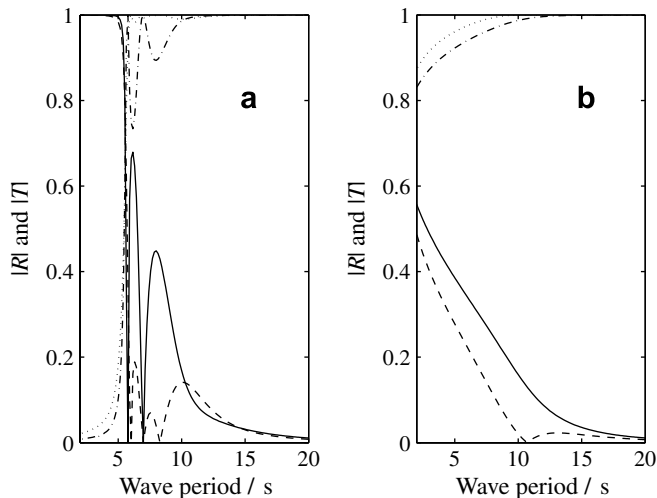


Fig. 3. As for Fig. 2 for a 20 m by 5-m-thick ice floe.

is treated properly. Each figure shows how an ice floe of 20 m width and a thickness different from the surrounding 1-m-thick ice sheet affects the passage of a flexural-gravity wave train. Both the reflection coefficient and the transmission coefficient are plotted, with parts (a) illustrating what happens when the edges of the ice floe are free, i.e. satisfy equation (3), and parts (b) designating a floe that is welded or frozen at its ends to the surrounding sheet, i.e. satisfies Eq. (4). It is evident that the frozen edge conditions on the right produce the simpler results and these will be discussed first.

In Fig. 2, the entrapped ice floe is 2 m thick, so there is a step of 0.1 m in freeboard and 0.9 m in draft associated with the floe. This produces a small increase in the reflection at all periods considered in part (b) and the removal of the zero at about 13.1 s in the no-submergence case where perfect transmission is predicted. Instead the $|R|$ curve monotonically decreases from a little above 0.4 at 2 s period to become negligible at long periods. The difference between the solid and the dashed curves is small but conspicuous (ca. 7%). However, in plotting the reflection coefficient we are exaggerating the effect, as we are actually most interested in how transmission is altered by the inclusion of draft when compared to the no-submergence solution because we are normally working out how much wave energy reaches the ice interior after it has passed through a number of obstacles. Since $|R|^2 + |T|^2 = 1$, differences between $|T|$ with draft included (dash-dot curve) and draft omitted (dotted curve) are actually only ca. 1% for periods less than 10 s and $|T| \approx 1$ with $< 0.2\%$ variation for longer waves.

In Fig. 3, the ice floe is 5 m thick, so the freeboard step is 0.4 m and the discontinuity in draft is 3.6 m at each edge of the entrapped 20-m-wide ice floe. Such dimensions would be considered typical of a fairly substantial pressure ridge, although the rectangular sectional shape is too simplistic of course. (Note, however, that in Fig. 4 of Williams and Squire (2004a) and the related discussion, different pressure

ridge shapes are shown to produce near identical results when correctly associated.) As expected, Fig. 3b is a more extreme version of Fig. 2b; again the no-submergence zero associated with perfect transmission is removed when draft is included and the solid curve sits a little above the dashed one. In this case, the difference at periods less than about 10 s is more significant for both $|R|$ (ca. 11%) and $|T|$ (ca. 5%) because of the considerable draft involved, but again effectively $|T| = 1$ for both curves above 10 s period where the curves are only ca. 1% apart at worst.

In Figs. 2a and 3a, the same comparison is done when the ends of the captured ice floe are free to move relative to the ice sheet and thus satisfy equation (3). Here the curves are much more complicated and both sets, i.e. submergence-free and submergence-included, have considerable fine structure associated with periods at which reflection is zero and transmission is perfect; the thicker case of Fig. 3a being a more extreme version of Fig. 2a. The inclusion of draft also causes local maxima and minima in $|R|$ to move period and a suggestion of a reduction in the number of periods at which perfect transmission occurs. While the amplifying effect of using $|R|$ is diminished in the plots of $|T|$, as discussed previously, there is still considerable fine structure evident in the $|T|$ curves at wave periods less than about 10 s, shown dash-dot (draft included) and dotted (no-submergence). Above 10 s for both the 2 m and 5 m ice floes cases, the curves converge rapidly to yield $|T| = 1$.

Fig. 4, reproduced from Williams and Squire (in press) and included here because it sets a context for the subsequent discussion, shows the effect of floe width, in this case for a 2-m-thick ice floe embedded in a 1-m-thick sea-ice

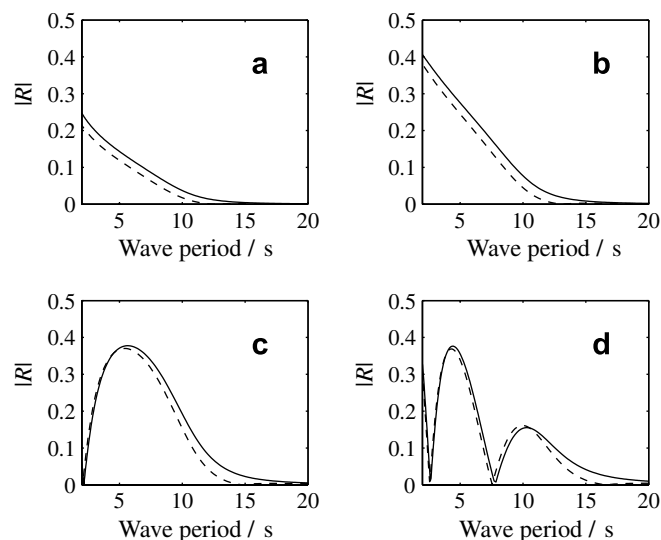


Fig. 4. The reflection coefficient R for a 2-m-thick ice floe floating on infinitely deep water between two semi-infinite 1 m thick sea-ice sheets, when submergence is allowed for (solid curves) and when it is not (dashed curves). The frozen edge conditions are applied and the floe widths used in each plot are (a) 10 m, (b) 20 m, (c) 50 m and (d) 100 m. (After Williams and Squire, in press.)

sheet. In each case the curves track one another well but note that their propinquity deteriorates at larger periods as the floe width is increased, i.e. in the sequence Fig. 4a–d. Recalling again the exaggerating effect of plotting $|R|$ as opposed to $|T|$, for the configurations shown the respective curves are pleasingly close being no more than about a few percent different throughout.

Although very long periods have not been included in Fig. 4 because the correspondence of the curves makes it impractical, observations suggest that well into the Arctic Ocean the ambient background swell is quite long (Hunkins, 1962). Furthermore, as one of the reviewers of the current paper points out, even though transmission may be very close to 100%, small relative changes in $|T|$ could be important, especially when integrated over a large number of features. Reassuringly, Table 1 confirms that the values of $|T|$ with and without submergence included are extremely close. The same effect seen in Fig. 4 is apparent, namely that broader features tend to emphasize differences, but the departure remains negligible and is certainly well within measurement error. It follows from these comparisons that the effect of draft on $|T|$ can be omitted to a good level of approximation—at least for thickness changes that are not too large and flexural-gravity waves typical of the ice-interior. Nonetheless, the accumulative effect of many irregular features could potentially deviate from that predicted by the no-submergence model when wave periods are modest, so this is now considered.

In Fig. 5, where the submergence (a) and no-submergence (b) cases are compared for 100 randomly defined ridges, we move a little closer to such a real ice field using statistical distributions provided by Wadhams (1988). Sail heights are drawn from an exponential distribution, sail widths follow by specifying a particular ridge geometry and ridge separations are chosen from a log-normal distribution. Both the wide spacing approximation developed in Section 2.3 and a serial approximation that neglects all but the principal transmitted wave train are plotted, with a 90% confidence interval shown dotted in each case. For both approximations but especially noticeable at longer periods, it is evident that the effect of including ridge drafts is to slightly increase the reflection coefficient by a few percent. Having said this the confidence interval band for the wide spacing approximation is broad and suggests the difference

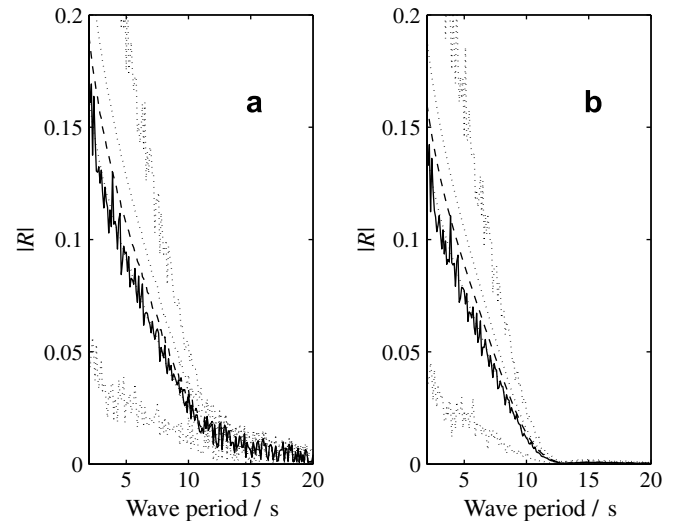


Fig. 5. The median wide-spacing (solid) and serial (dashed) approximations used to compare a heterogeneous ice sheet composed of 100 pressure ridges, with draft correctly included (a) and with no submergence (b). The sail height and separation of each ridge are drawn from an exponential distribution and a log-normal distribution respectively. Thickness is found assuming that the ice is in isostatic equilibrium and width follows by assuming all ridges have the same simple shape. Confidence intervals are shown dotted.

is not always statistically significant. The median wide-spacing results normally fall inside the confidence interval of the serial approximation and so for simplicity subsequent results are presented using the latter.

In all cases the $|R|$ curve drops monotonically from its value at low periods to become very small above about 10 s, but the cases representing the serial approximation (dashed) are much less noisy than those for the wide spacing approximation proper (solid) because in the former case *reverberation* of waves between ridges in the medium does not occur. In interpreting Fig. 5 the relationship $|R|^2 + |T|^2 = 1$ must also be kept in mind as before, since this will tend to suppress differences between an ice sheet where draft is correctly included and one where it is absent.

Randomly selected ridges and leads are both included in Fig. 6 in the arbitrarily chosen ratio 50:50, where the general shape of the solid (draft included) and dashed (no-submergence) curves is the same. Ridges are chosen as in Fig. 5, while lead widths and separations are respectively drawn

Table 1

Difference between the magnitude of the transmission coefficient $|T|$ with and without draft included for wave periods in the range 30–100 s and floe widths of 10, 20, 50 and 100 m

	10 m	20 m	50 m	100 m
30 s	3.4092×10^{-8}	1.4542×10^{-7}	6.7436×10^{-7}	2.2878×10^{-6}
35 s	1.5213×10^{-8}	8.1493×10^{-8}	3.6076×10^{-7}	1.1695×10^{-6}
40 s	7.7826×10^{-9}	5.2407×10^{-8}	2.2320×10^{-7}	6.9713×10^{-7}
45 s	4.3479×10^{-9}	3.6698×10^{-8}	1.5105×10^{-7}	4.5551×10^{-7}
50 s	2.5803×10^{-9}	2.7209×10^{-8}	1.0871×10^{-7}	3.1716×10^{-7}
75 s	2.8615×10^{-10}	9.4926×10^{-9}	3.4488×10^{-8}	8.8698×10^{-8}
100 s	1.5991×10^{-11}	4.6535×10^{-9}	1.6158×10^{-8}	3.8632×10^{-8}

The table extends Fig. 4 to selected long periods.

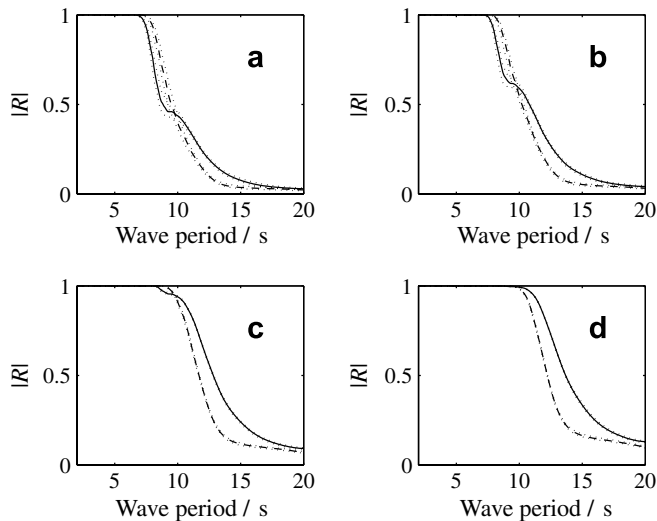


Fig. 6. The serial approximation used to compare a heterogeneous ice sheet composed of (a) 50, (b) 100, (c) 500 and (d) 1000 ridges and leads (50% of each), with draft correctly included (solid) and with no submergence (dashed). 90% confidence intervals are shown dotted and are very close to the median curves.

from a power law distribution and an exponential one. As usual, dashed curves denote no submergence and solid curves properly include the draft. The curves are separated slightly in parts (a–d) and, in fact, cross over when the number of features is not large, i.e. in Fig. 6a–c, at an intermediate period of ca. 10 s and at a much longer period. (The curves actually also cross in Fig. 6d but this occurs where $|R| \approx 1$ effectively.) This is due to the presence of the leads, which tend to have a significantly greater impact on the waves than do ridges—presumably because they are associated with free edge conditions (3) rather than welded edge conditions (4). An equivalent plot to Fig. 6 with leads alone shows basically the same shape, while that for ridges alone has no cross overs. Interestingly, when a semi-infinite sheet is modelled, i.e. open water for $-\infty < x < 0$ and sea-ice for $0 \leq x < \infty$, the same cross over occurs (see Fig. 8 of Williams and Squire, in press). Reasons for the cross over are subtle—as wavelength is altered by including draft, although it is clear that at short periods the inclusion of draft will offer an effective barrier to wavelengths not too much greater than the submergence, while at very long periods the waves will not tend to see the difference for the relatively small draft involved. The behaviour in between was not anticipated by the authors.

The cross overs are certainly interesting but recall that the number of features in Fig. 6a–c is quite small; for the 1000 ridges and leads appearing in Fig. 6d the behaviour is much simpler. Essentially, because the cross overs occur when $|R| \approx 1$ and as $|R| \rightarrow 0$, the inclusion of draft always effectively causes increased reflection and, accordingly, less transmission. Draft effects are apparently quite significant at intermediate periods, even with the effect of the relationship $|R|^2 + |T|^2 = 1$, which tends to diminish their contribution to the forward propagating wave train. However,

recalling that only very long waves can penetrate and survive in the deep Arctic Ocean interior and noting that the two curves become less easily discriminated above ca. 20 s period, the inclusion of draft in mathematical models may be geophysically extraneous in this setting. This confirms our hunch about the importance of draft to $|R|$ and $|T|$ at longer periods, which was discussed earlier in relation to an extrapolation of Fig. 4. Because the volatility associated with the multiple reflections that occur in the precise and wide spacing approximation is removed in the serial approximation, the confidence interval is narrow and the distinction between the curves is meaningful.

4. Geophysical implications

The primary geophysical aim of this paper has been to establish whether the correct inclusion of draft is important in calculating the progression of waves through isolated abrupt features such as ridges and leads in a continuous ice cover, and across an ice field composed of many such features. To do this we have focused upon R , the reflection coefficient, recognizing that effects on T , the transition coefficient, are suppressed through the relationship $|R|^2 + |T|^2 = 1$ and that plots of $|T|$ tend to smear out detail. Before summarizing the results in terms of their geophysical implications, however, we present a plot arising from Fig. 6 that shows how a Pierson–Moskowitz wave spectrum (Pierson and Moskowitz, 1964) would change after progressing through 50, 100, 500 or 1000 ridges and leads. Alternatively Fig. 7 may be perceived as showing

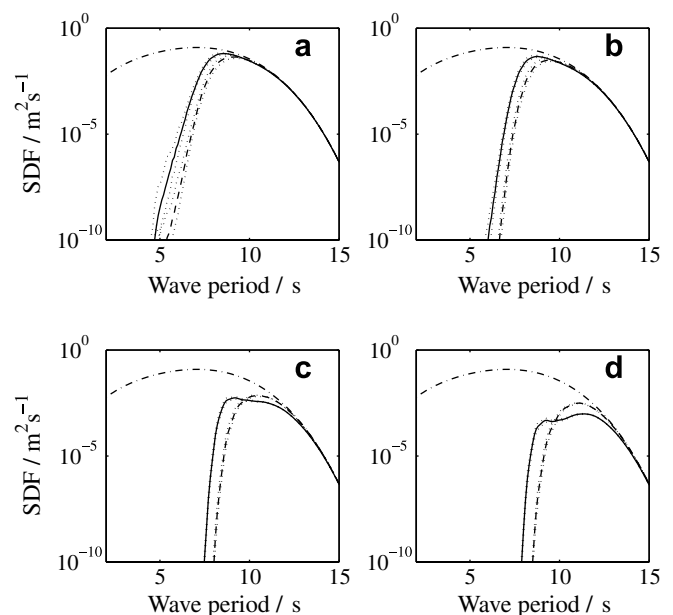


Fig. 7. Evolution of a Pierson–Moskowitz spectrum (dot-dash curve) through an ice field composed of equal proportions of ridges and leads drawn from the same statistics distributions as in Fig. 6, for (a) 50, (b) 100, (c) 500 and (d) 1000 features. Solid curves show what happens when draft is included, while dashed curves are for when it is omitted. Confidence intervals are shown dotted.

how the spectrum evolves as it penetrates further into an ice cover, i.e. fetch and quantity of features are interchangeable, and we have deliberately plotted the ordinate spectral density function axis logarithmically to emphasize this interpretation rather than allowing each part to be rescaled. Granting this means that the usual shape of the Pierson–Moskowitz spectrum is less familiar, we feel it improves the interpretation. Note that the energy density is also plotted against wave period as opposed to frequency. This is to avoid the compression that occurs at longer periods with the latter mode of plotting and for compatibility with the earlier figures. Despite previous papers by the authors having investigated how wave spectra proceed through ice fields, e.g. Williams and Squire (2004b), because of the geophysical value of such information to the processes by which ice fields change and its importance to ships and marine structures such as hydrocarbon rigs in ice infested waters, no prior analysis has been done that includes Archimedean draft for the hydroelastic ice floes present.

At all penetrations quite large differences are evident between the ice covers with draft included and those without when the wave period is less than about 12 s or so. Yet it is not simply a case of saying that the inclusion of draft causes greater attenuation, as the cross overs discussed in relation to Fig. 6 begin to play a role. For example, after 50 features in Fig. 7a greater attenuation of the incoming spectrum is predicted when submergence is omitted than when it is included because the Pierson–Moskowitz spectrum has most of its energy occurring between about 5 and 10 s. The same behaviour is evident in Fig. 7b, but in Fig. 7c for 500 features, a distinct cross over appears at ca. 10 s that separates similar behaviour at low periods from a range of periods where including draft causes more energy to be removed from the passing waves. This pattern continues for Fig. 7d, where 1000 features have affected the spectrum. Here, the no-submergence spectrum (dashed) is actually significantly larger above 10 s than the case with draft included (solid)—up to ca. three times the energy density, although the logarithmic plot does not accentuate this especially well.

To finish our discussion of Fig. 7 we state the obvious, namely that ridges and leads influence the passage of flexural-gravity waves as they progress further into sea-ice. The overall energy in the spectrum is diminished preferentially, with greater attenuation occurring at low periods than at long periods, so spectral shape is a function of penetration. The correct inclusion of draft does alter the degree to which the spectrum distorts, not because the transmission coefficients are markedly different in each case but more because of accumulated contributions from many such differences. Differences are most pronounced at short periods and, in fact, because only long wavelengths survive the passage into the ice interior, the effect of draft is less of an issue there. Unfortunately, no field data exist that can confirm the accuracy of Fig. 7 and such an experiment would be very difficult to do because of the requirement to character-

ize fully and accurately the geometry of every feature present.

Since large areas of the central Arctic Ocean and the Southern Ocean away from the continent and Peninsula are relatively free of massively deformed sea-ice, models that do not include draft would appear to be satisfactory in many cases for reproducing how waves travel through fields of sea-ice as most of the short period wave energy will have been dissipated en route. Accordingly, current models that apply the boundary conditions for single features at the mean water line, e.g. Balmforth and Craster (1999), Chakrabarti (2000), Squire and Dixon (2000, 2001a,b), Sahoo et al. (2001), Linton and Chung (2003), Porter and Porter (2004), Chung and Linton (2005), Manam et al. (2006) and Williams and Squire (2006, 2007), will provide a good description of what is actually occurring in nature and may, with care, potentially be extended to connect many such features together.

While our goal has been to investigate the effect of draft, its inclusion has created a much more robust model of continuous heterogeneous sea-ice, with its many irregularities correctly incorporated. Bennetts et al. (2007) and Williams and Squire (in press) have each independently developed mathematical theory that allows individual features to be properly represented and, in principle, we may combine these features to investigate ice fields of considerable extent and inhomogeneity. We have shown how to do this using the Williams and Squire work by means of a wide spacing approximation that neglects the effect of evanescent waves on adjacent features and a serial approximation that neglects reverberation. Such models are becoming increasingly important as climate warming begins to be felt, in terms of both the observed and anticipated increases in extreme weather events—including storms, and the metamorphosis of sea-ice into a physically weaker state that is more easily destroyed by waves due to warmer temperatures. Storms are likely to be accompanied by intensified ocean wave activity, which will penetrate further into the sea-ice veneer from the open sea and will break it up more readily by a variety of mechanisms including enhanced flexural-gravity-wave-induced stressing. With the ability to produce plots of spectral evolution such as Fig. 7 for physically-realistic heterogeneous ice sheets, we are in a position to compute whether or not sea-ice at any particular location will fracture using methods such as those described by Langhorne et al. (1998, 2001). In this scenario, the wave energy density at any position in the sea-ice field will be found, allowing the strain at that location to be compared with that required for fracture—possibly taking into account fatigue as described by Langhorne et al. (2001). By this means, the ice field will gradually evolve to steady state with no changes of external forcing, recalling that, as the distribution of floe sizes and thickness changes, so too will the spatial distribution of the wave energy across the ice cover. Over and above an increased prevalence of storms and weaker sea-ice, a warmer Earth will potentially have further attendant effects. For example, we expect and

are already observing more open water in the form of leads and polynyas, e.g. the 100,000 sq km per year ice cover reduction over the last 10 years in the Arctic, culminating in 2007 in a 1 million sq km drop and the opening of the Northwest Passage (Pedersen, 2007) so the overall concentration will be less and ocean waves will penetrate further into the ice interior. The process we are describing will have a significant impact as the air/sea-ice/ocean fluxes will alter markedly as positive feedback leads to continued growth in the open water fraction present over vast areas of the polar seas.

A final comment relates to an interesting repercussion of the current work to the solution of the inverse problem. That is, can waves be used as a remote sensing agent to determine the properties of an ice sheet? This idea is not new and in fact goes back to D. Ye. Kheysin, but to date it has not been fully tested. Kheysin's idea, developed by Nagurny et al. (1994), is to tune quite subtle features in the solution of a floating uniform thin elastic plate to find a mean sheet thickness. While imaginative, the current authors feel that the efficacy of the thin plate model is being pushed to extremes by such an approach. Although a parsimonious theory such as this would be extremely useful, we prefer the current approach whereby the sea-ice terrain is modelled to the best of our ability and the results are then tuned to match observations. Having said this, both approaches may drive valuable field programmes that will complement the significant theoretical developments that have occurred over the last decade. While the authors are really just at the start of using waves in this way, some progress has been made (Williams, 2005; Vaughan and Squire, 2006; Vaughan et al., 2007; Vaughan and Squire, 2007) and we expect to continue to develop these ideas towards a functional tool that will extract sea-ice properties from remotely sensed wave information.

Acknowledgements

V.A.S. and T.D.W. are supported by the University of Otago and by the Marsden Fund Council from Government funding administered by the Royal Society of New Zealand. The authors acknowledge useful comments made by anonymous reviewers.

References

- Andrianov, A.I., Hermans, A.J., 2005. Hydroelastic analysis of floating plate of finite draft. In: Grue, J. (Ed.), Proceedings 20th International Workshop on Water Waves and Floating Bodies. University of Oslo, Oslo, Norway <<http://www.iwwfb.org/Workshops/20.htm>>.
- Balmforth, N.J., Craster, R.V., 1999. Ocean waves and ice sheets. *J. Fluid Mech.* 395, 89–124.
- Barrett, M., Squire, V.A., 1996. Ice-coupled wave propagation across an abrupt change in ice rigidity, density or thickness. *J. Geophys. Res.* 101 (C9), 20825–20832.
- Bennetts, L.G., Biggs, N.R.T., Porter, D., 2007. A multi-mode approximation to wave scattering by ice sheets of varying thickness. *J. Fluid Mech.* 579, 413–443.
- Berry, M.V., Klein, S., 1997. Transparent mirrors: rays, waves and localization. *Eur. J. Phys.* 18 (3), 222–228.
- Bishop, R.E.D., Price, W.G., 1979. *Hydroelasticity of Ships*. Cambridge University Press, Cambridge.
- Bishop, R.E.D., Price, W.G., Wu, Y., 1986. A general linear hydroelasticity theory of floating structures moving in a seaway. *Philos. T. Roy. Soc. A* 316 (1538), 375–426.
- Chakrabarti, A., 2000. On the solution of the problem of scattering of surface-water waves by the edge of an ice cover. *Proc. R. Soc. Lon. Ser-A* 456 (1997), 1087–1099.
- Chou, T., 1998. Band structure of surface flexural-gravity waves along periodic interfaces. *J. Fluid Mech.* 369, 333–350.
- Chung, H., Fox, C., 2002. Propagation of flexural-gravity waves at the interface between floating plates. *Int. J. Offshore Polar* 12 (3), 163–170.
- Chung, H., Linton, C.M., 2005. Reflection and transmission of waves across a gap between two semi-infinite elastic plates on water. *Q. J. Mech. Appl. Math.* 58 (1), 1–15.
- Comiso, J., 2002. A rapidly declining perennial sea-ice cover in the Arctic. *Geophys. Res. Lett.* 29 (20), 1956. doi:10.1029/2002GL015650.
- Eatock Taylor, R., 2003. Wet or dry modes in linear hydroelasticity – why modes? In: Eatock Taylor, R. (Ed.), Proceedings of 3rd International Conference on Hydroelasticity in Marine Technology. University of Oxford, Oxford, UK, pp. 239–250.
- Eatock Taylor, R., 2007. Hydroelastic analysis of plates and some approximations. *J. Eng. Math.* 58 (1–4), 267–278.
- Evans, D.V., Davies, T.V., 1968. Wave-ice interaction. Tech. Rep. 1313, Davidson Laboratory, Stevens Institute of Technology, New Jersey.
- Evans, D.V., Porter, R., 2003. Wave scattering by narrow cracks in ice sheets floating on water of finite depth. *J. Fluid Mech.* 484, 143–165.
- Fox, C., Squire, V.A., 1990. Reflection and transmission characteristics at the edge of shore fast sea ice. *J. Geophys. Res.* 95, 11629–11639.
- Fox, C., Squire, V.A., 1991. Coupling between an ocean and an ice shelf. *Ann. Glaciol.* 15, 101–108.
- Fox, C., Squire, V.A., 1994. On the oblique reflexion and transmission of ocean waves from shore fast sea ice. *Philos. T. Roy. Soc. A* 347 (1682), 185–218.
- Hermans, A.J., 2007. Free-surface wave interaction with a thick flexible dock or very large floating platform. *J. Eng. Math.* 58 (1–4), 77–90.
- Hunkins, K., 1962. Waves on the Arctic Ocean. *J. Geophys. Res.* 67 (6), 2477–2489.
- Kohout, A.L., Meylan, M.H., 2006. A model for wave scattering in the marginal ice zone based on a two-dimensional floating elastic plate solution. *Ann. Glaciol.* 44, 101–107.
- Kreisel, G., 1949. Surface waves. *Q. Appl. Math.* 7, 21–44.
- Langhorne, P.J., Squire, V.A., Haskell, T.G., 1998. Breakup of sea ice by ocean waves. *Ann. Glaciol.* 27, 438–442.
- Langhorne, P.J., Squire, V.A., Haskell, T.G., 2001. Lifetime estimation for a fast ice sheet subjected to ocean swell. *Ann. Glaciol.* 33, 333–338.
- Linton, C., McIver, P., 2001. *Handbook of Mathematical Techniques for Wave/Structure Interactions*. CRC Press, Boca Raton, FL.
- Linton, C.M., Chung, H., 2003. Reflection and transmission at the ocean/sea-ice boundary. *Wave Motion* 38 (1), 43–52.
- Manam, S.R., Bhattacharjee, J., Sahoo, T., 2006. Expansion formulae in wave structure interaction problems. *Proc. R. Soc. Lon. Ser-A* 462 (2065), 263–287.
- Marchenko, A.V., 1997. Flexural gravity wave diffraction at linear irregularities in sheet ice. *Fluid Dyn.* 32 (4), 548–560.
- Meylan, M.H., 1993. The behaviour of sea ice in ocean waves. Ph.D. thesis, University of Otago, Dunedin, New Zealand.
- Meylan, M.H., Squire, V.A., 1994. The response of ice floes to ocean waves. *J. Geophys. Res.* 99 (C1), 899–900.
- Meylan, M.H., Squire, V.A., 1996. Response of a circular ice floe to ocean waves. *J. Geophys. Res.* 101 (C4), 8869–8884.
- Meylan, M.H., Squire, V.A., Fox, C., 1997. Toward realism in modelling ocean wave behaviour in marginal ice zones. *J. Geophys. Res.* 102 (C10), 22981–22991.
- Mindlin, R.D., 1951. Influence of rotatory inertia and shear on flexural motions of isotropic elastic plates. *J. Appl. Mech.* 18, 31–38.

- Nagurny, A.P., Korostolev, V.G., Abaza, V.P., 1994. A method for determination of effective sea ice thickness in the Arctic basin for climate monitoring. *Bull. Russ. Acad. Sci. Phys. Suppl. Phys. Vib.* 58, 168–174.
- Newman, J.N., 1977. *Marine Hydrodynamics*. MIT Press, Cambridge, MA.
- Newman, J.N., 1994. Wave effects on deformable bodies. *Appl. Ocean Res.* 16 (1), 47–59.
- Pedersen, L.T., 14th September 2007. European Space Agency Portal. <http://www.esa.int/esaCP/SEMYYTC13J6F_index_0.html>.
- Peter, M.A., Meylan, M.H., Linton, C.M., 2006. Water-wave scattering by a periodic array of arbitrary bodies. *J. Fluid Mech.* 548, 237–256.
- Pierson, W.J., Moskowitz, L., 1964. A proposed spectral form for fully developed wind seas based on the similarity theory of S.A. Kitaigorodskii. *J. Geophys. Res.* 69, 5181–5190.
- Porter, D., Porter, R., 2004. Approximations to wave scattering by an ice sheet of variable thickness over undulating bed topography. *J. Fluid Mech.* 509, 145–179.
- Rothrock, D.A., Yu, Y., Maykut, G.A., 1999. Thinning of the Arctic sea-ice cover. *Geophys. Res. Lett.* 26 (23), 3469–3472.
- Sahoo, T., Yip, T.L., Chwang, A.T., 2001. Scattering of surface waves by a semi-infinite floating elastic plate. *Phys. Fluids* 13 (11), 3215–3222.
- Sarpkaya, T., Isaacson, M., 1981. *Mechanics of Wave Forces on Offshore Structures*. Van Nostrand Reinhold, New York.
- Squire, V.A., 2007. Of ocean waves and sea-ice revisited. *Cold Reg. Sci. Technol.* 49 (2), 110–133.
- Squire, V.A., Dixon, T.W., 2000. An analytic model for wave propagation across a crack in an ice sheet. *Int. J. Offshore Polar* 10 (3), 173–176.
- Squire, V.A., Dixon, T.W., 2001a. How a region of cracked sea ice affects ice-coupled wave propagation. *Ann. Glaciol.* 33, 327–332.
- Squire, V.A., Dixon, T.W., 2001b. On modelling an iceberg embedded in shore fast sea ice. *J. Eng. Math.* 40 (3), 211–236.
- Squire, V.A., Dugan, J.P., Wadhams, P., Rottier, P.J., Liu, A.K., 1995. Of ocean waves and sea ice. *Annu. Rev. Fluid Mech.* 27, 115–168.
- Tkacheva, L.A., 2001. Scattering of surface waves by the edge of a floating elastic plate. *J. Appl. Mech. Tech. Phys.* 42 (4), 638–646.
- Tkacheva, L.A., 2002. Diffraction of surface waves at floating elastic plate. In: Rainey, R.C.T., Lee, S.F. (Eds.), *Proceedings of the 17th International Workshop on Water Waves and Floating Bodies*. The Royal Institution of Naval Architects, Cambridge, England <<http://www.iwwfb.org/Workshops/17.htm>>.
- Tkacheva, L.A., 2004. The diffraction of surface waves by a floating elastic plate at oblique incidence. *J. Appl. Math. Mech.* 68 (3), 425–436.
- Vaughan, G.L., Squire, V.A., 2006. Scattering of ice-coupled waves by variable sea-ice terrain. *Ann. Glaciol.* 44, 88–94.
- Vaughan, G.L., Squire, V.A., 2007. Scattering of ice-coupled waves by a sea-ice sheet with random thickness. *Wave Random Complex* 17 (3), 357–380.
- Vaughan, G.L., Williams, T.D., Squire, V.A., 2007. Perfect transmission and asymptotic solutions for reflection of ice-coupled waves by inhomogeneities. *Wave Motion* 44 (5), 371–384.
- Wadhams, P., 1988. Sea ice morphology. In: Lepparanta, M. (Ed.), *Physics of Ice Covered Seas*, vol. 1. Helsinki University Printing House, Finland, pp. 231–287.
- Wadhams, P., Davis, N.R., 2000. Further evidence of ice thinning in the Arctic Ocean. *Geophys. Res. Lett.* 27 (24), 3973–3976.
- Williams, T.D., 2005. Reflections on ice: the scattering of flexural-gravity waves by irregularities in Arctic and Antarctic ice sheets. Ph.D. thesis, University of Otago, Dunedin, New Zealand.
- Williams, T.D., Squire, V.A., 2002. Wave propagation across an oblique crack in an ice sheet. *Int. J. Offshore Polar* 12 (3), 157–162.
- Williams, T.D., Squire, V.A., 2004a. Oblique scattering of plane flexural-gravity waves by heterogeneities in sea ice. *Proc. R. Soc. Lon. Ser-A* 460 (2052), 3469–3497.
- Williams, T.D., Squire, V.A., 2004b. The scattering of flexural-gravity waves by an ice field. *Int. J. Offshore Polar* 14 (3), 161–168.
- Williams, T.D., Squire, V.A., 2006. Scattering of flexural-gravity waves at the boundaries between three floating sheets with applications. *J. Fluid Mech.* 569, 113–140.
- Williams, T.D., Squire, V.A., 2007. Wave scattering at the sea-ice/ice-shelf transition with other applications. *SIAM J. Appl. Math.* 67 (4), 938–959.
- Williams, T.D., Squire, V.A., in press. The effect of submergence on wave scattering across a transition between two floating flexible plates. *Wave Motion*.
- Wu, C., Watanabe, E., Utsunomiya, T., 1995. An eigenfunction expansion-matching method for analyzing the wave-induced responses of an elastic floating plate. *Appl. Ocean Res.* 17 (5), 301–310.